(Received 17 November 2025, Accepted 31 December 2025, Scheduled 28 January 2026)

Novel Ovate Antenna for Wireless Communication: Characteristic Mode and Time Domain Analyses

Elisha Chand* and Sellakkutti Suganthi

Christ University, Bangalore 560084, Karnataka, India

ABSTRACT: In this article, a novel ovate-shaped microstrip antenna (OMSA) is presented for the application in wireless communication. It covers the evolution of a new shape and delves deeper into the resonance mechanism of the proposed design using characteristic mode analysis (CMA). The OMSA resonates at 2.45 GHz and 2.69 GHz with the return loss of -18.82 dB and -31.84 dB, respectively. It offers an ultra-wideband performance with 91.46% measured bandwidth. The characteristic impedance and VSWR at 2.4 GHz are 49 Ω and 1.3, respectively. By introducing performance enhancement techniques such as ground truncation and a notch in the patch, the antenna resonance characteristics have been enhanced. A prototype of the proposed OMSA has been fabricated and validated experimentally. The time domain characteristics of the proposed OMSA have been simulated for both face-to-face (FtF) and side-by-side (SbS) configurations. The FtF configuration offers better performance, showcasing the group delay of the OMSA $<$ 2 ns and minimal variation along the operating band. The phase linearity is also maintained, minimizing any distortions. The time domain results demonstrate a maximum fidelity factor of 90.62%, reaffirming the suitability of the antenna for wireless communication. The suitability of the proposed OMSA for wireless applications is also validated experimentally by analyzing the group delay and S_{21} phase linearity of the received signal.

1. INTRODUCTION

Microstrip antennas (MSAs) have become essential in wireless communications due to their low profile, lightweight structure, and ease of integration with printed circuit boards and active circuits. They are widely deployed in applications such as WLAN [1–3], WBAN [4, 5], Bluetooth [6–8], and ISM-band devices [9–11] to count a few.

However, conventional MSAs are notoriously narrowband. It may limit their application in contemporary applications. In order to keep up with the evolving technological pace, novel MSAs must cater to multiple applications and even support high data rates. By efficiently tweaking the MSA design parameters, the performance of the MSA can be controlled.

Bandwidth (BW) and resonance enhancement techniques, such as truncated ground, incorporation of slots and notches, novel radiator geometries, and defected ground structures (DGSs), have been shown to significantly improve the BW performance. For example, the BW performance of a novel hexagon-shaped patch geometry is able to achieve an ultra-wideband (UWB) BW by incorporating a ribbon-shaped slot in the patch [12]. Additionally, regular antenna shapes have demonstrated wideband performance by simply modifying the ground plane [13]. Using fractal shapes along with a modified ground plane increases the effective electrical length of the antenna, contributing to better resonance and UWB performance [14]. Antennas of other novel shapes like hook-shape [15], ψ-shape [16], or even Yin-yang-shape [17] demonstrate wide BW performance while maintaining the aesthetic appeal and creativity. Current reviews also emphasize the effect of metamaterials [18, 19], slotting, and geometry optimization [20, 21] techniques in achieving impedance matching and gain enhancement across multiple sub-bands. The antenna's design parameters, along with specific absorption rate (SAR) analysis, were discussed in the previous work. This work discusses the mechanism and effect of various performance enhancement techniques used at each antenna evolution stage.

The MSA performance evaluation largely focuses on frequency-domain performance metrics such as BW, gain, and voltage standing wave ratio (VSWR). Time-domain characteristics, such as fidelity factor, pulse distortion, and group delay linearity, have received less attention for wideband antennas and are mainly discussed for UWB applications. These metrics are critical for ensuring minimal signal distortion, efficient pulse transmission, and improved system performance. Thus, this work shows both frequency and time domain analysis of a novel ovate-shaped antenna operating in 2.2 GHz to 6 GHz band. Along with WLAN, Bluetooth, and Wi-Fi, the antenna effectively covers both 2.45 GHz and 5 GHz for Industrial, Scientific, and Medical (ISM) applications. In order to validate the proposed antenna's suitability for wireless communication applications, parameters like group delay (GD), phase linearity (PL), and fidelity factor (FF) have been evaluated.

This manuscript holistically covers the OMSA design evolution, its simulation, and experimental validation, along with suitability in prospective applications. The design evolution and parametric optimization are covered in Section 2. The section also covers the impact of performance enhancement techniques on the OMSA's resonance performance. Later in Sec-

* Corresponding author: Elisha Chand (chandelisha@gmail.com).

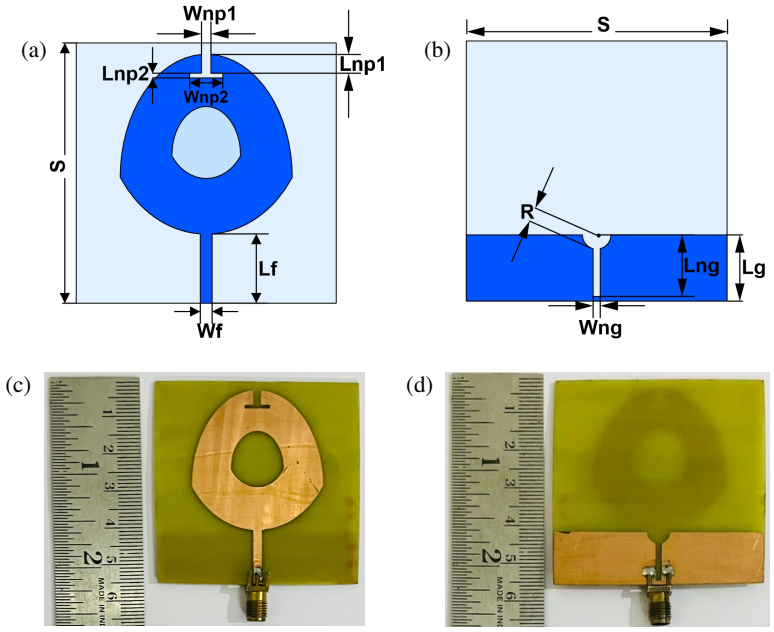

FIGURE 1. Proposed OMSA schematic representation, (a) top side, (b) bottom side and fabricated prototype, (c) top side, (d) bottom side.

tion 3, the measured results are compared with the simulated ones. The results are also compared with other state-of-the-art antennas found in recent literature. Section 3 deals with the antenna performance in WLAN and WBAN applications. The simulation results in the application scenario are analyzed and discussed. This manuscript concludes with a reiteration and reaffirmation of the OMSA's overall performance in Section 4.

The theory of characteristics mode is an effective computational method that is used to understand the resonant behavior of a conducting structure. The theory was first proposed by Grabacz and Turpin [22] and later formalized by Harrington and Mautz [23, 24]. It performs full-wave analysis of the integral electric field equations using Method of Moments (MoM). Over time, characteristic mode analysis (CMA) has evolved into a powerful method to comprehend the resonance of an antenna and, in turn, leverage this to enhance its characteristics like bandwidth (BW), gain, radiation pattern, and even polarization [25–27].

This manuscript employs CMA to delve deeper into the numerical interpretation of the antenna's resonance behavior through its evolution stages. The UWB performance of the antenna, along with its suitability for wireless communication, is experimentally validated. Time-domain characteristics, such as fidelity factor, pulse distortion, and group delay linearity, are critical for ensuring minimal signal distortion, efficient pulse transmission, and improved system performance. Thus, this work shows both frequency and time domain analysis of a novel ovate-shaped antenna operative in 2.2 GHz to 6 GHz band. Along with WLAN, Bluetooth, and Wi-Fi, the antenna effectively covers both 2.45 GHz and 5 GHz for ISM applications. In order to validate the proposed antenna's suitability in wireless communication applications, parameters like group delay (GD), phase linearity (PL), and fidelity factor (FF) have been evaluated. The UWB performance of the antenna, along with its suitability for wireless communication, is experimentally validated. Time-domain characteristics, such as fidelity factor, pulse distortion, and group delay linearity, are critical for ensuring minimal signal distortion, efficient pulse transmission, and improved system performance. Thus, this work shows both frequency and time domain analysis of a novel ovate-shaped antenna operative in 2.2 GHz to 6 GHz band. Along with WLAN, Bluetooth, and Wi-Fi, the antenna effectively covers both 2.45 GHz and 5 GHz for ISM applications. In order to validate the proposed antenna's suitability in wireless communication applications, parameters like GD, PL, and FF have been evaluated.

2. ANTENNA DESIGN EVOLUTION

A novel ovate antenna operative in 2.2 GHz to 6 GHz band is presented in this section. The shape of the radiator is inspired by the ovate shape of leaves. The ground plane and radiator have been modified to enhance the resonance characteristics. The antenna was designed on a 55 mm × 55 mm FR-4 substrate ($\varepsilon_r = 4.4$, $h = 1.6$ mm). In order to explore the future use as arrays, the antenna is fed using a 2.5 mm wide microstrip feed line. The antenna evolution stages and dimensions are shown in Fig. 1 and Table 1, respectively. The impact of all variations is analyzed using the current distribution maps and S_{11} characteristics, which are illustrated in Fig. 3 and Fig. 4, respectively.

All the evolutionary stages are depicted in Fig. 2(a). In the first A0 stage, an ovate patch antenna (OPA) is created by taking inspiration from the ovate shape of leaves. It is the preliminary stage, as seen in Fig. 2(b), and resonates at 5.7 GHz. To enhance the resonance characteristics, the full ground plane of the OPA was truncated to nearly one-fourth of the original length. This is antenna A1. The A1 antenna resonates at 2.7 GHz, and wideband performance was observed. By introducing truncation in the ground plane of the antenna, the current distribution changes, making the antenna resonate in the

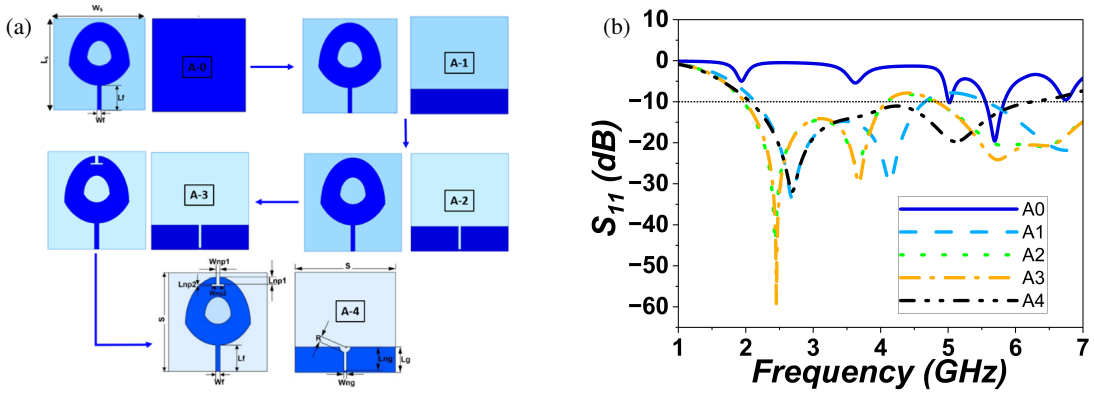

FIGURE 2. Simulation of evolutionary stages of the OMSA.

TABLE 1. Dimensions of the proposed OMSA.

Design Parameter	Dimension (mm)
Side of square substrate S	55
Height of substrate h	1.6
Length of ground plane L_g	14
Length of feed L_f	15
Width of feed W_f	2.5
Length of ground notch L_{ng}	13
Width of ground notch W_{ng}	1.5
Length of 1st patch notch L_{np1}	4
Width of 1st patch notch W_{np1}	2
Length of 2nd patch notch L_{np2}	1
Width of 2nd patch notch W_{np2}	3.5
Radius of semi-circular notch R	3

desired band. Notches are an effective way for fine-tuning the resonant frequency and impedance matching. A notch can alter the current path and adjust the electrical length of the antenna without changing the overall footprint of the antenna. Thus, to further enhance the resonance characteristics, a notch of size $L_{ng} \times W_{ng}$ was introduced in the ground plane, the next stage A2. With the introduction of the notch, the resonance reached 2.45 GHz at -43 dB. In the next stage, A3, the resonance characteristics are enhanced more with the help of a T-shaped notch along the length of the patch. The dimensions of the vertical hand of the T-slot are $L_{np1} \times W_{np1}$, and those of the horizontal hand are $L_{np2} \times W_{np2}$. The introduction of this notch enhances the return loss value of the antenna. Finally, the final A4 antenna is created by adding a semicircular notch of radius R. With the introduction of this notch, the BW of the antenna becomes UWB from 2 GHz to 6 GHz.

Therefore, this antenna is finalized for fabrication. This final A4 evolution stage and the hereafter is referred to as OPA. The final design specifications of the A4 OPA are mentioned in Table 1. In stage II (A1), the ground plane is truncated to create additional resonances. This is well supported by the evolutionary stages III (A2) and IV (A4). The S_{11} at 2.45 GHz improves from -10 dB in stage II to -15 dB and -23 dB in these respective stages. The notches introduced in the ground and patch show better S_{11} response at the resonant frequency. Now, to tackle the concern of widening the impedance bandwidth, the ground plane is further modified by adding a semicircular cut-out notch to the already existing rectangular notch. With the introduction of semicircular notch, the antenna resonance slightly shifts to 2.6 GHz, but it exhibits a wideband behavior from 2.2 GHz to 6 GHz. This A4 antenna is the proposed novel ovate MSA, which is referred to as OMSA in the subsequent sections. For further CMA analysis, only stages A1–A4 will be considered as they resonate at the desired frequency of 2.45 GHz.

3. CHARACTERISTIC MODE ANALYSIS

The CMA is a systematic, physics-based approach that explains the electromagnetic behavior by decomposing the antenna's surface current into orthogonal characteristic modes. This surface current density [22–24] can be expressed in the form of eigen-currents.

$$\vec{J} = \sum\nolimits_n \frac{V_n^i}{1 + j\lambda_n} J_n \tag{1}$$

where J_n is the eigen-current determined purely by the shape of the conductor and is called the modal weight coefficient (MWC). The modal excitation coefficient (MEC) is denoted by V_n^i and is a measure of how strongly the applied excitation gets coupled to the conductor. The ratio of stored to radiated energy is given by the eigenvalue λ_n. Even though λ_n can take values in the range $(-\infty, \infty)$, the mode is said to be resonant when $\lambda_n = 0$. The stored magnetic field becomes dominant when $\lambda_n > 0$, and the mode is said to be inductive. The mode is capacitive when $\lambda_n < 0$ and the stored electric field is dominant.

For very large values of λ_n, the resonance is determined by modal significance (MS). A mode's contribution to the total response at a frequency is given by its MS. For resonance, MS $= 1$, and the band for which $1 \leq \text{MS} \leq 0.707$ is the modal bandwidth.

$$\text{MS} = \left| \frac{1}{1 + j\lambda_n} \right| \tag{2}$$

The phase difference between J_n and tangential electric field component is given by characteristic angle α_n. The mode is

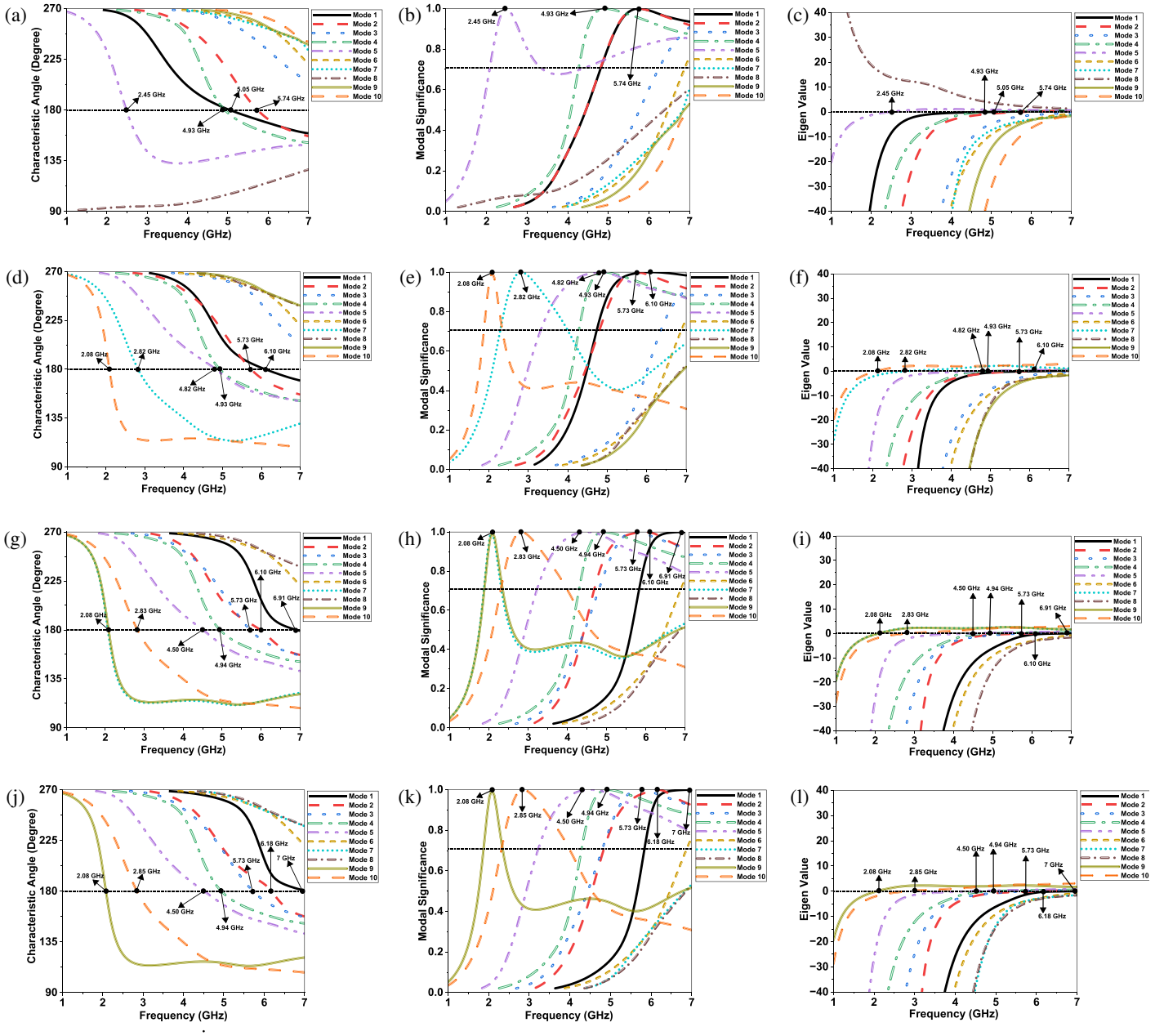

FIGURE 3. CMA of the OMSA evolution stages, (a) α_n for stage A1, (b) MS for stage A1, (c) λ_n for stage A1, (d) α_n for stage A2, (e) MS for stage A2, (f) λ_n for stage A2, (g) λ_n for stage A3, (h) α_n for stage A3, (i) MS for stage A4, (j) λ_n for stage A4, (k) α_n for stage A4, (l) MS for stage A3.

resonant at $\alpha_n = 180°$, inductive for $90° < \alpha_n < 180°$ and capacitive for $180° < \alpha_n < 270°$.

$$\alpha_n = 180° - \tan^{-1}(\lambda_n) \tag{3}$$

The plots for α_n, MS, and λ_n for the evolutionary stages of the antenna are illustrated in Fig. 3. To perform CMA, only conducting surfaces of the antenna are considered in simulation, and the CMA was performed for 10 modes. In A1 stage, four modes are found to resonate. Mode-1 resonates at 4.93 GHz; Mode-2 resonates at 5.74 GHz; Mode-4 resonates at 4.93 GHz; and Mode-5 resonates at 2.45 GHz. While Mode-8 is capacitive in nature, all the other modes are inductive. Thus, the addition of capacitive loading can help enhance the BW. With the introduction of a capacitive slot in the ground plane at the A2 stage, the number of resonant modes increases, and the BW is enhanced. Modes 1 and 2 in A2 closely follow each other and resonate at 6.10 GHz and 5.73 GHz, respectively. Modes 4, 5, and 10 resonate at 4.82 GHz, 2.82 GHz, and 2.08 GHz, respectively. All the other modes are inductive in nature. To enhance the resonance and BW, a capacitive slot is incorporated in the patch. The number of modes is further increased to 8 in the A3 stage. Mode-1 resonates at 6.91 GHz, and Mode-2 resonates 6.10 GHz. An additional Mode-3 resonates at 5.73 GHz. Modes 4 and 5 resonate at 4.94 GHz and 4.50 GHz, respectively. Modes 7 and 9 overlap at 2.08 GHz, and Mode-10 resonates at 2.83 GHz. While the resonance at 2.45 GHz is significantly enhanced in this stage, it can be seen that the BW is nearly the same. This can be attributed to the

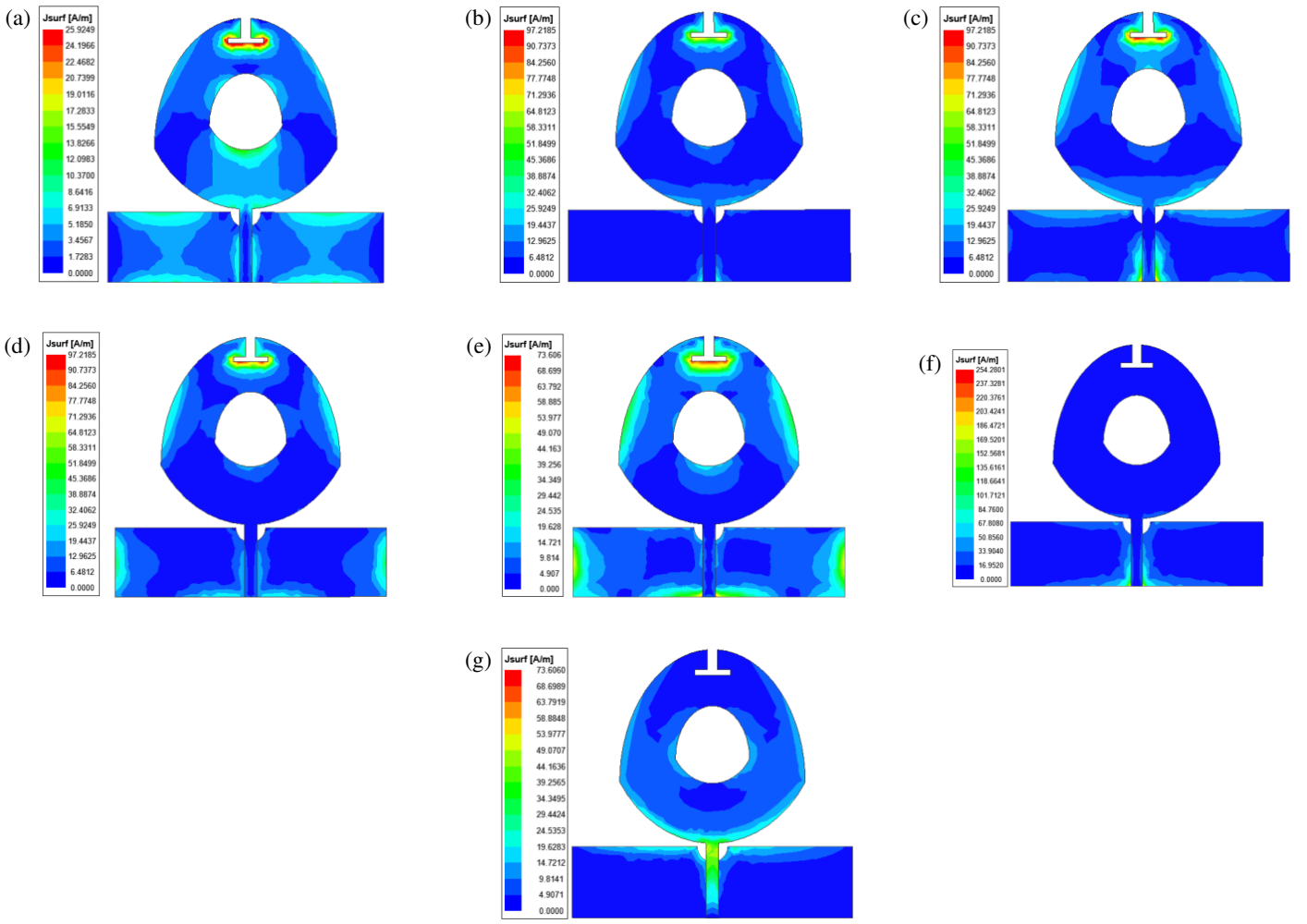

FIGURE 4. Modal current distributions at (a) Mode-1 at 7 GHz, (b) Mode-2 at 6.18 GHz, (c) Mode-3 at 5.73 GHz, (d) Mode-4 at 4.94 GHz, (e) Mode-5 at 4.50 GHz, (f) Mode-9 at 2.08 GHz and (g) Mode-10 at 2.85 GHz.

overlap of Modes 7 and 9. Even though the number of modes increases, the modes are not spaced far enough to have a significant influence on the BW. Other modes are still inductive in the range of interest. Thus, a capacitive semi-circular notch is added in the final A4 stage. With the addition of this notch, 7 out of the 10 modes resonate distinctly. Modes 1–5 resonate at 7 GHz, 6.18 GHz, 5.73 GHz, 4.94 GHz, and 4.50 GHz, respectively. Modes 9 and 10 contribute to resonance at lower frequencies at 2.85 GHz and 2.08 GHz, respectively. The current distributions, along with the 2D radiation patterns for all resonant modes in A4 stage, are shown in Fig. 4 and Fig. 5, respectively. This OMSA is then fabricated and analyzed for the applications in wireless communication.

4. RESULTS AND DISCUSSION

A prototype of the proposed OMSA has been fabricated, as shown in Fig. 1(b) and measured to validate its performance. All simulations have been done using Ansys HFSS and MATLAB, whereas all the measurements for validation have been made at a defense-based laboratory for antenna testing in Jodhpur, India, using the art Vector Network Analyzer (VNA) and testing facilities. Both frequency and time domain analyses (FDA and TDA) have been evaluated in this manuscript.

4.1. Frequency Domain Performance

In this work, the antenna shows a slight variation in the simulated and measured results. This is highly due to fabrication tolerances and the soldering issue with the connector. However, the antenna shows a UWB performance in both simulation and measurement.

While UWB communication is primarily discussed in the 3.1 GHz to 10.6 GHz range, the fundamental UWB definition is based on BW. According to this definition, an antenna with an absolute BW greater than 500 MHz or fractional BW (FBW) greater than 20% is essentially falling under the UWB range [28]. As seen in Fig. 6(a), the antenna effectively resonates at 2.45 GHz with 101.45% simulated FBW and 91.46% measured FBW. Thus, the antenna is UWB. The OMSA is well matched with both simulated and measured VSWR < 2 and characteristic impedance $(Z_0) \approx 50\,\Omega$ in the entire operational range. It has a measured VSWR of 1.2 at 2.6 GHz with characteristic impedance of 49 Ohms. The simulated and measured VSWRs and Z_0 are illustrated in Figs. 6(b) and (c), respectively.

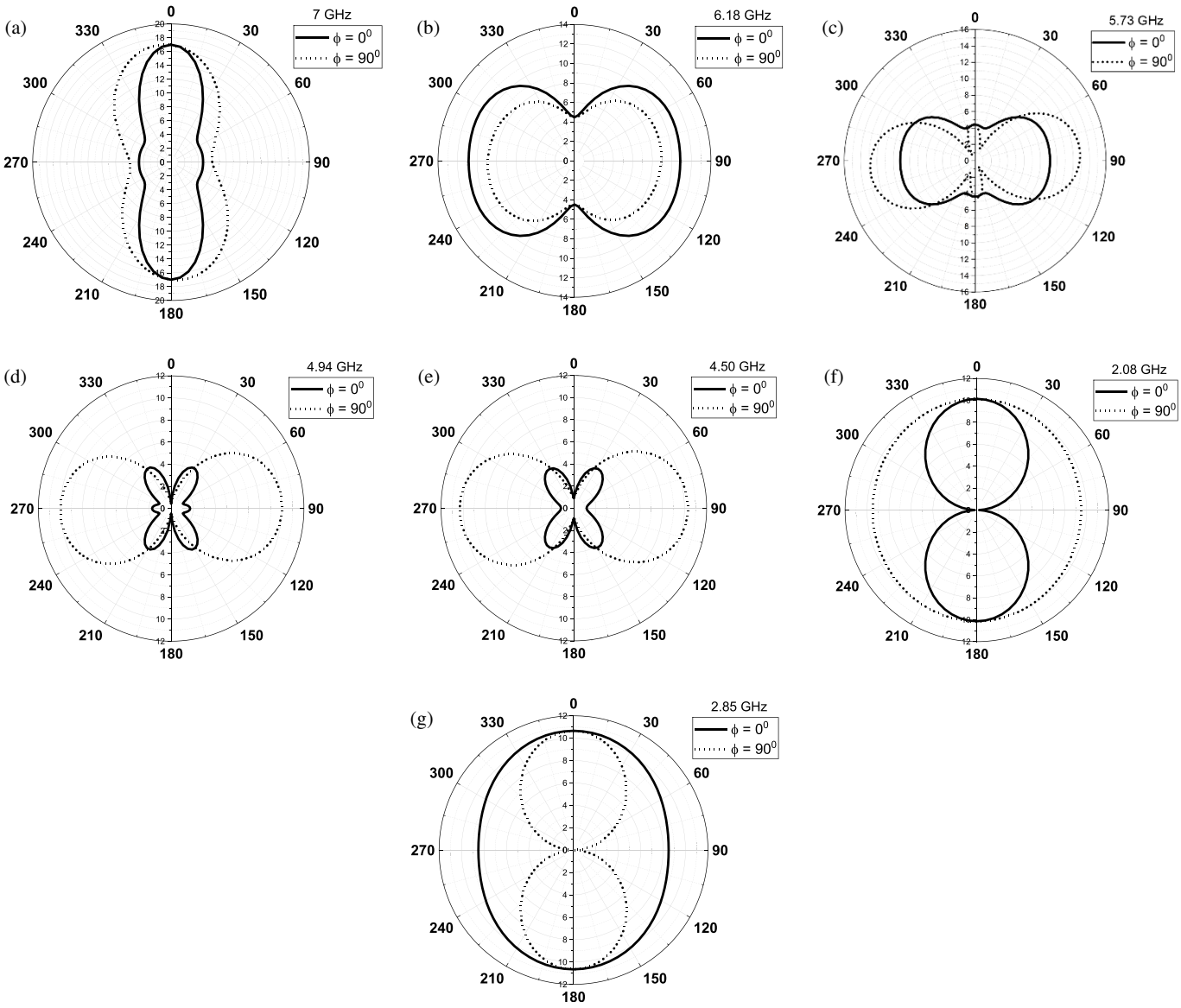

FIGURE 5. Radiation patterns at $\phi = 0^\circ$ and $\phi = 90^\circ$ for (a) Mode-1 at 7 GHz, (b) Mode-2 at 6.18 GHz, (c) Mode-3 at 5.73 GHz, (d) Mode-4 at 4.94 GHz, (e) Mode-5 at 4.50 GHz, (f) Mode-9 at 2.08 GHz and (g) Mode-10 at 2.85 GHz.

The normalized E- and H-plane gains and radiation patterns (RPs) of the antenna are compared in Fig. 6(d). The antenna has an omnidirectional radiation in the H-plane. The truncation of ground plane has resulted in a back-lobe, making the OMSA radiation bidirectional in the E-plane. The simulated half-power beamwidth (HPBW) in the E-plane is 78.9°. The measured HPBW in this plane slightly decreases to 58.6°. Even though the antenna is omnidirectional in the H-plane, a slight HPWB of 34.4° is observed. The RPs, however, align maximally in both planes, validating the OMSA's performance.

The gain of the OMSA has been measured in free space outside of an anechoic chamber for a more realistic estimate in a noisy environment. The measured gain is depicted in Fig. 6(e). The peak measured gain at 2.45 GHz is 4.5 dB. The simulation trends comply maximally with the measured results in the frequency domain. Any digressions can be attributed to connector soldering and fabrication tolerances.

4.2. Time Domain Performance

The feasibility of the OMSA for signal transmission through short pulses is verified by performing TDA. This is done by simulating a wireless communication link. The designed OMSA is used as a transmitter and receiver. The antennas are placed 350 mm away from each other, enabling far-field signal transmission. Two different configurations were simulated, whereas the antennas are facing each other (FtF) and side by side (SbS). The transmitted input pulse is prone to distortion at the receiver because of its susceptibility to losses and dispersion. Therefore, the TDA of the transmitted pulse is necessary to mitigate distortion concerns.

The fidelity factor (FF), group delay (GD), and phase linearity (PL) are effective parameters to gauge the antenna's performance in the time domain. The calculation of FF [29] gives similarity or correlation between the transmitted and received signals. The input and output signals are first normalized, and

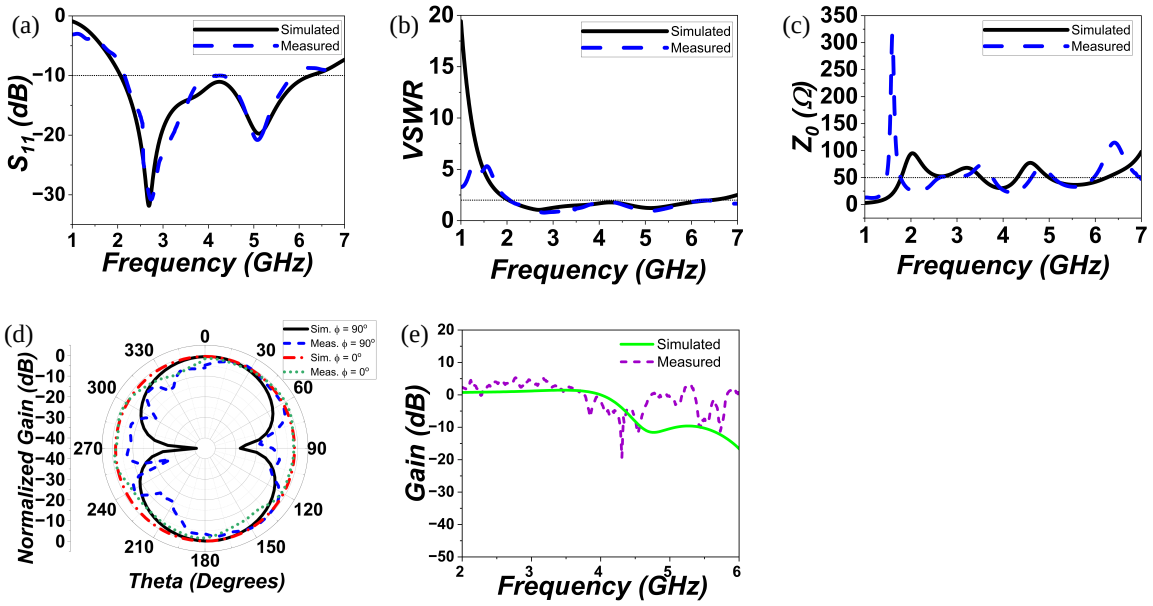

FIGURE 6. Comparison of simulated and measured results of the OMSA, (a) S_{11} characteristics, (b) VSWR, (c) characteristic impedance, (d) normalized radiation patterns at 2.45 GHz, (e) gain vs frequency.

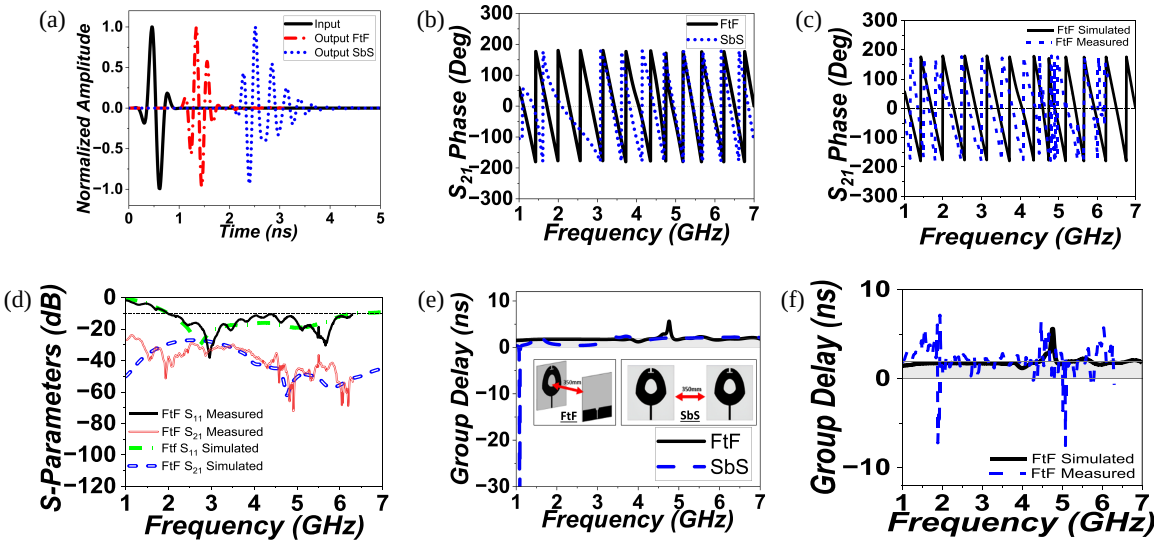

FIGURE 7. Results of OMSA for wireless communication applications, (a) simulated normalized transmitted and received waveforms, (b) simulated S_{21} phase linearity, (c) simulated and measured S_{21} phase linearity for FtF, (d) simulated and measured S-parameters for FtF, (e) group delays for FtF and SbS, (f) simulated and measured group delay for FtF.

then the cross-correlation between them is computed.

$$\mathrm{FF} = \max\left\{\frac{\int_{-\infty}^{\infty} T(t)\, R(T-\tau)\, dt}{\sqrt{\int_{-\infty}^{\infty}\left|T(t)^2\right| dt \int_{-\infty}^{\infty}\left|R(t)^2\right| dt}}\right\} \quad (4)$$

Since the FF depends on both the antenna specifications and excitation signal, it is important to choose a suitable input. The input pulse should be chosen such that its pulse spectrum falls almost entirely within the antenna's operational bandwidth [30]. The simulated normalized input and output signals are shown in Fig. 7(a). The FF ranges between 0 and 1. A value of 0 indicates maximum distortion and minimum correlation. While the FF should be as close to 1 as possible, values > 0.5 are also deemed acceptable. The transmitted and received pulses for the Ftf and SbS scenarios are shown in Fig. 7(c). The FF for FtF is 0.9062 (or 90.62%) and for SbS 0.0051 (or 51%. This indicates that the antenna performs well, and the transmitted signal is received with minimal distortions. Although the acceptable range is FF $> 50\%$, the FtF configuration is more suitable for establishing communication without compromising signal integrity.

In order to ensure distortion-free transmission, GD and PL are also analyzed. The GD [30] describes a negative rate of change of phase (φ) with respect to the change in angular fre-

TABLE 2. Comparison of proposed OMSA with other designs in literature.

Reference Antenna	Dimensions (mm)	Frequency Range (GHz)	% BW	Gain (dB)
[31]	42 × 32	2.67∼3.40 3.61∼3.67	24.09% 1.64%	3.69
[32]	30 × 30	2.42–2.50	3.25%	4.1
[33]	20 × 30	2.43–2.64 3.02–3.85 4.88–6.82	8.30% 24.19% 33.16%	1.8
[34]	50 × 50	2.48–6.7	91.9%	2.78
[35]	143.5 × 227.5	0.5–5.5	166.66%	2.6
[36]	40 × 34	2.26–4.10 6.0–9.82	57.86%	2.5
[37]	50 × 50	1.595–1.958 3.164–3.55	20.50% 11.64%	2.09
[38]	48 × 38	2.16–2.85 4.8–5.96	27.8% 21.5%	2.55
Proposed Work	**55 × 55**	**2.14–5.88 (measured)**	**93.3%**	**4.5**

quency (ω)

$$\text{GD} = \frac{-d\varphi}{d\omega} \tag{5}$$

Ideally, GD response should be flat and nearly constant throughout the frequency range of operation with minimal deviations. As seen in Figs. 7(b)–(f), the GD and PL vary minimally with minimal distortions in the FtF scenario.

This indicates that the distortions are more for the SbS than for the FtF scenario. The PL response is also stable with minimal distortions for the entire frequency range in the FtF configuration. The GD is well within the acceptable range of < 2 ns with a few additional disturbances in the SbS configurations. This signifies that the received pulse has minimal to no out-of-phase components. The measured frequency domain results of the proposed OMSA are compared with other designs available in the literature in Table 2.

Since all the designs taken for comparison are based on a 1.6 mm thick FR-4 substrate, the dimensions are only the length and width. While antennas other than [30] are smaller in size than the proposed OMSA, their BW is significantly less as well. On the other hand, while [30] offers better BW, its size and gain are significant setbacks. The proposed OMSA offers UWB performance while maintaining a comparable size.

5. CONCLUSION

In this article, the design and analysis of a novel OMSA, along with the time and frequency domain performance, have been extensively presented. This work offers an in-depth analysis of the key drivers of the antenna performance. The antenna performance is enhanced using intricate techniques such as truncated ground, notches in the ground and patch. The effect of each stage is analyzed by the antenna's current distribution and RL characteristics. The simulated and measured performances show satisfactory impedance matching and wide BW. The normalized RPs in both E- and H-planes also aligned maximally. For TDA, crucial performance parameters like FF, GD, and PL are simulated. While GD and PL have been measured, the measurement and analysis of FF may be explored in future studies. The simulated time domain performance showcases high fidelity values for the FtF configuration. The novelty of the OMSA is its distinctive shape, in-depth resonance performance analysis using CMA, experimental verification of both time and frequency domain responses using state-of-the-art measurement facilities, and comparison with the existing antenna designs. Hence, the proposed OMSA is recommended for wireless communication, including WLAN applications.

REFERENCES

[1] Chung, M.-A., M.-C. Lee, C.-C. Hsu, and C.-W. Lin, "Multi-band coupled-fed antenna for 4G LTE, Sub-6G, and WLAN frequency bands in various electronic devices," *IEEE Access*, Vol. 12, 45 398–45 422, 2024.

[2] Sakulchat, S., A. Ruengwaree, W. Naktongq, P. Unahalekhaka, and S. Promput, "Low-cost high gain sea pimp-shaped dual band monopole antenna for mobile 4G/5G/LTE41/WLAN application," *Progress In Electromagnetics Research C*, Vol. 140, 41–51, 2024.

[3] Khan, M. A., W. T. Sethi, W. A. Malik, A. Jabbar, M. A. Khalid, A. M. Almuhlafi, and M. Himdi, "A comprehensive analysis of low-profile dual band flexible omnidirectional wearable antenna for WBAN applications," *IEEE Access*, Vol. 12, 45 187–45 201, 2024.

[4] Du, J., R. Wang, H. Li, X.-X. Yang, and C. Roblin, "All-textile compact ultra-wideband microstrip antenna with full ground plane for WBAN applications," *International Journal of Antennas and Propagation*, Vol. 2024, No. 1, 4236695, 2024.

[5] Khan, N. H. N., B. Feng, X. Ding, W. Gu, L. Deng, and K. L. Chung, "Dual-band printed antenna design for Bluetooth and

WLAN applications," in *2024 IEEE 7th International Conference on Electronic Information and Communication Technology (ICEICT)*, 1122–1125, Xi'an, China, 2024.

[6] Vuyyuru, S. K. R., M. Räsänen, J. H. S. Bergman, and J. Holopainen, "Design and validation of a compact dual-band Bluetooth antenna for smartwatch applications," in *2025 19th European Conference on Antennas and Propagation (EuCAP)*, 1–5, Stockholm, Sweden, 2025.

[7] Yu, Z., R. Sun, G. Zhang, R. Niu, X. Ran, and Z. Lin, "A flexible wearable antenna with annular solar eclipse structure for ISM/WLAN/WIMAX/Bluetooth applications," *International Journal of Antennas and Propagation*, Vol. 2023, No. 1, 8969565, 2023.

[8] Tong, X., J. Xu, H. Zhang, and X. Yu, "An integrated microwave and millimeter-wave circularly polarized antenna with ISM band gain suppression performance," *IEEE Antennas and Wireless Propagation Letters*, Vol. 23, No. 11, 3649–3653, Nov. 2024.

[9] Cai, H. and C. Liu, "Circularly polarized loop antenna for 2.4 GHz ISM-band biotelemetry devices," *IEEE Antennas and Wireless Propagation Letters*, Vol. 24, No. 2, 509–513, Feb. 2025.

[10] Singh, S. and S. Verma, "Compact dual band and dual polarized CPW-fed triangular shaped wearable antenna for ISM band applications," *Electromagnetics*, Vol. 42, No. 1, 38–50, 2022.

[11] Park, S. and K.-Y. Jung, "Novel compact UWB planar monopole antenna using a ribbon-shaped slot," *IEEE Access*, Vol. 10, 61 951–61 959, 2022.

[12] Chavali, V. A. P. and A. A. Deshmukh, "Wideband designs of regular shape microstrip antennas using modified ground plane," *Progress In Electromagnetics Research C*, Vol. 117, 203–219, 2021.

[13] Karad, K. V., V. S. Hendre, J. L. Rajput, V. Kadam, V. E. Narawade, R. Bakale, and G. D. Londhe, "A SAR analysis of hexagonal-shaped UWB antenna for healthcare applications," *EURASIP Journal on Wireless Communications and Networking*, Vol. 2024, No. 72, 2024.

[14] Swetha, R. and L. Anjaneyulu, "Novel design and characterization of wide band hook shaped aperture coupled circularly polarized antenna for 5G application," *Progress In Electromagnetics Research C*, Vol. 113, 161–175, 2021.

[15] Deshmukh, A. A. and A. A. Odhekar, "Dual band circularly polarized modified Ψ-shape microstrip antenna," *Progress In Electromagnetics Research C*, Vol. 115, 161–174, 2021.

[16] Feng, B., S. Qi, X. Ding, X. Yang, and C.-Y.-D. Sim, "A dual-polarized multi-wideband ceiling antenna with eight-diagram shape for 2G/3G/LTE/5G Sub-6 GHz indoor applications," *IEEE Access*, Vol. 12, 135 338–135 351, 2024.

[17] Du, C., L.-R. Pei, J. Zhang, and C.-X. Shi, "A gain enhanced dual-band low SAR AMC-based MIMO antenna for WBAN and WLAN applications," *Progress In Electromagnetics Research M*, Vol. 115, 21–34, 2023.

[18] Wang, F., Y. Wang, X. Zhang, L. Liu, K. Li, and Y. Ren, "Wideband low-RCS and gain-enhanced antenna using frequency selective absorber based on patterned graphene," *Scientific Reports*, Vol. 14, No. 1, 9306, 2024.

[19] Reddy, R. N., N. V. K. Rao, and D. R. Krishna, "An AMC-backed dual-band gain-enhanced wearable antenna with low SAR for WLAN/WBAN applications," *Progress In Electromagnetics Research C*, Vol. 146, 55–64, 2024.

[20] Kumar, A. and G. P. Pandey, "A narrow beam gain enhanced wideband antenna array using slits, I-slots, and L-shaped reflector for 5G millimeter wave applications," *International Journal of RF and Microwave Computer-Aided Engineering*, Vol. 2024, No. 1, 8919125, 2024.

[21] Kamil, A. Q., H. M. Kadhim, and R. M. Alsammarraie, "Gain improvement for single band ultra-wideband antenna by slots technique," in *2024 21st International Multi-Conference on Systems, Signals & Devices (SSD)*, 755–760, Erbil, Iraq, 2024.

[22] Garbacz, R. and R. Turpin, "A generalized expansion for radiated and scattered fields," *IEEE Transactions on Antennas and Propagation*, Vol. 19, No. 3, 348–358, 1971.

[23] Harrington, R. and J. Mautz, "Theory of characteristic modes for conducting bodies," *IEEE Transactions on Antennas and Propagation*, Vol. 19, No. 5, 622–628, 1971.

[24] Harrington, R. and J. Mautz, "Computation of characteristic modes for conducting bodies," *IEEE Transactions on Antennas and Propagation*, Vol. 19, No. 5, 629–639, 1971.

[25] Mohammad, A. and A. Hassan, "Dual-wideband MIMO antenna using characteristic mode theory for mobile terminal applications," *IEEE Access*, Vol. 13, 138 914–138 931, 2025.

[26] Thotakura, H., R. Gogineni, K. S. Rao, C. K. Kumar, R. B. Sadineni, and S. Mandava, "A miniaturized highly isolated two port triple band-notched UWB MIMO antenna verified by characteristic mode analysis," *Progress In Electromagnetics Research C*, Vol. 160, 133–142, 2025.

[27] Wang, Z., F. Zhang, W. Nie, M. Yang, and C. Li, "A racket-shaped UWB MIMO antenna based on characteristic mode analysis," *Progress In Electromagnetics Research B*, Vol. 114, 37–50, 2025.

[28] Federal Communications Commission, "47 CFR §15.503 — Definitions," Code of Federal Regulations, Title 47, Part 15, Subpart F (Ultra-Wideband Operation), U.S. Government Publishing Office, Washington, DC, [Online]. https://www.ecfr.gov/current/title-47/chapter-I/subchapter-A/part-15/subpart-F/section-15.503, 2025.

[29] Mobashsher, A. T. and A. M. Abbosh, "Compact 3-D slot-loaded folded dipole antenna with unidirectional radiation and low impulse distortion for head imaging applications," *IEEE Transactions on Antennas and Propagation*, Vol. 64, No. 7, 3245–3250, Jul. 2016.

[30] Simorangkir, R. B. V. B., A. Kiourti, and K. P. Esselle, "UWB wearable antenna with a full ground plane based on PDMS-embedded conductive fabric," *IEEE Antennas and Wireless Propagation Letters*, Vol. 17, No. 3, 493–496, Mar. 2018.

[31] Hasan, M. M., M. R. I. Faruque, and M. T. Islam, "Dual band metamaterial antenna for LTE/Bluetooth/WiMAX system," *Scientific Reports*, Vol. 8, No. 1, 1240, 2018.

[32] Gautam, A. K., M. Farhan, N. Agrawal, and K. Rambabu, "Design and packaging of a compact circularly polarised planar antenna for 2.45-GHz RFID mobile readers," *IET Microwaves, Antennas & Propagation*, Vol. 13, No. 13, 2310–2314, 2019.

[33] Sharma, N., A. Kumar, A. De, and R. K. Jain, "Design of compact hexagonal shaped multiband antenna for wearable and tumor detection applications," *Progress In Electromagnetics Research M*, Vol. 105, 205–217, 2021.

[34] Benkhadda, O., S. Ahmad, M. Saih, K. Chaji, A. Reha, A. Ghaffar, S. Khan, M. Alibakhshikenari, and E. Limiti, "Compact broadband antenna with vicsek fractal slots for WLAN and WiMAX applications," *Applied Sciences*, Vol. 12, No. 3, 1142, 2022.

[35] Amirinalloo, S. and Z. Atlasbaf, "A CPW-fed fractal monopole antenna with a reduced ground plane in frequency range of 500 MHz–5.5 GHz," *IET Microwaves, Antennas & Propagation*, Vol. 17, No. 13, 1006–1014, 2023.

[36] Marzouk, M., Y. Rhazi, I. H. Nejdi, F.-E. Zerrad, M. Saih, S. Ahmad, A. Ghaffar, and M. Hussein, "Ultra-wideband compact

fractal antenna for WiMAX, WLAN, C and X band applications," *Sensors*, Vol. 23, No. 9, 4254, 2023.

[37] Yassen, M. T., A. J. Salim, M. R. Hussan, and J. K. Ali, "A compact dual-band dual-polarized antenna based on modified Minkowski fractal," *Progress In Electromagnetics Research C*, Vol. 140, 11–19, 2024.

[38] Lamultree, S., N. Somsanook, W. Narkkoht, and C. Phongcharoenpanich, "A dual-band rectangular shape incorporated into circular patch antenna for 2.4/5 GHz wireless local area network applications," *TELKOMNIKA (Telecommunication Computing Electronics and Control)*, Vol. 23, No. 1, 22–31, 2025.